Plasmonics (2012) 7:143–150
DOI 10.1007/s11468-011-9287-3

The Role of Propagating and Localized Surface Plasmons for SERS Enhancement in Periodic Nanostructures

Francisco J. Bezares · Joshua D. Caldwell · Orest Glembocki · Ronald W. Rendell · Mariya Feygelson · Maraizu Ukaegbu · Richard Kasica · Loretta Shirey · Nabil D. Bassim · Charles Hosten

Received: 9 June 2011 / Accepted: 8 September 2011 / Published online: 20 September 2011

Abstract Periodic arrays of plasmonic nanopillars have been shown to provide large, uniform surface-enhanced Raman scattering (SERS) enhancements. We show that these enhancements are the result of the combined impact of localized and propagating surface plasmon modes within the plasmonic architecture. Here, arrays of periodically arranged silicon nanopillars of varying sizes and interpillar gaps were fabricated to enable the exploration of the SERS response from two different structures; one featuring only localized surface plasmon (LSP) modes and the other featuring LSP and propagating (PSP) modes. It is shown that the LSP modes determine the optimal architecture, and thereby determine the optimum diameter for the structures at a given incident. However, the increase in the SERS enhancement factor for a system in which LSP and PSP cooperatively interact was measured to be over an order of magnitude higher and the peak in the diameter dependence was significantly broadened, thus, such structures not only provide larger enhancement factors but are also more forgiving of lithographic variations.

F. J. Bezares (✉) · J. D. Caldwell · O. Glembocki · R. W. Rendell · M. Feygelson · L. Shirey · N. D. Bassim
US Naval Research Laboratory,
4555 Overlook Ave, S.W.,
Washington, DC 20375, USA
e-mail: francisco.bezares.ctr@nrl.navy.mil

M. Ukaegbu · C. Hosten
Chemistry Department, Howard University,
Washington, DC 20059, USA

R. Kasica
Center for Nanoscale Science and Technology,
National Institute for Standards and Technology,
Gaithersburg, MD 20899, USA

Keywords SERS · Surface plasmons · E-beam lithography · Molecular detection · Plasmonics

Introduction

Surface plasmon (SP), which are collective oscillations of electrons near the surface of a metal, came into prominence because of surface-enhanced Raman scattering (SERS), which was initially reported in the 1970s by Fleishman and was later explained by Jeanmarie and Van Duyne [1, 2]. SERS allowed for the detection of submonolayer chemical coverages on nanotextured Au or Ag in systems which normally would have been insensitive to such low molecular densities [3]. As a result, this motivated extensive research in recent decades and have sparked the development of plasmonic superlenses [4, 5], plasmon-enhanced solar cells [6, 7], and plasmonic metamaterials [8], while the properties of SP have also been exploited to provide electromagnetic (EM) field enhancements that enabled more efficient emitters as well as single molecule detection via SERS [9–11]. This broad range of applications are mainly due to the electro-optical properties of SP and can be categorized into two different types; localized surface plasmon (LSP) or propagating surface plasmon (PSP). PSP can be defined as propagating EM waves bound between metal/dielectric interfaces. In the case of LSP, the EM waves, and consequently surface electrons in the metal, are confined to small areas relative to the wavelength of the incident excitation. While the properties of each, LSP and PSP, are desired for particular applications such as SERS and electro-optical waveguiding, respectively, the combination of the properties of both could result in further advancements in plasmonic device technology. For instance, in the case of LSP, a high degree of localization of

the EM near-fields near the surface of a nanostructure can be achieved, leading to large detection enhancements of optical signals. On the other hand, for the case of PSP, highly efficient waveguiding of EM energy as well as information across a device can be obtained [12–14]. Thus, combining the properties of LSP and PSP and manipulating the interactions between them could also lead to the development of novel applications that require the retention and transport of EM energy and information such as in ultrafast and ultradense computing [15–17].

Basic plasmonic nanostructures like metallic nanoparticles or nanopillars can generally support LSP [15], while PSP are typically created at the surface of a metal film, extended hole arrays such as extraordinary transmission gratings or waveguide structures [14, 18]. In other words, whether the SP modes of a nanostructure are localized or propagating will be strongly dependent upon the geometry and dimensions of that structure. More complex (hybrid) nanostructures with architectures combining different geometries and dimensions may exhibit characteristics attributable to both types of SP and their resulting interactions [15, 19, 20]. Chu and Crozier [21] reported that the near-field spectra of a device consisting of a Au nanodisk array, a SiO_2 spacer, and a Au thin film shows the characteristic resonances for modes belonging to the PSP of the Au thin film as well as the LSP of the Au nanodisks. In their experiment, they showed how the evanescent near-fields are enhanced by the interaction with the Au nanodisks and its image charge and they claimed that the near-fields of the system are further enhanced by the interaction between the two modes. Further studies by Mock et al. [22] illustrated the interaction between LSP confined to Au colloids and PSP within an underlying Au film with a dielectric spacer layer.

In this study, we investigate the interaction between LSP and PSP in two different sets of nanopillar arrays. We show that an increase in SERS enhancement factor of 1–2 orders of magnitude can be attained by combining LSP and PSP within a given architecture. For our work, we used Si nanopillar arrays similar to those reported previously by our group [23] where both a Au cap over the top surface of the nanopillars and a Au film throughout the area between their base are present and compared these to similar nanopillar arrays, where only the Au cap was present, thus eliminating the source of any PSP modes. In the context of the work we report here, we take PSP to encompass SP polariton waves confined to the Au-air and Au-Si interfaces, as well as the SP that develop at the air gap between the Au film and the base of the Si nanopillars. EM simulations provided further insight into the interaction mechanism and illustrate the importance of this combination.

Materials and Methods

Nanopillar Array Fabrication

Each of the two nanopillar structures studied here consisted of a full-factorial set of nanopillar arrays which, prior to Au deposition (Si only), featured diameters extending from 87 to 288 nm and interpillar gaps, defined as the edge-to-edge distance between the sidewalls of adjacent nanopillars on a given row or column, ranging from 86 to 298 nm. Each of the nanopillar arrays consisted of a 100×100 square lattice of Si nanopillars. The bare Si nanopillar height on the two samples was measured to be approximately 170 nm.

The samples were fabricated by patterning a thin poly (methyl methacrylate) layer via electron-beam (e-beam) lithography using a 100-kV VISTEC system. Metal deposition was carried out using an e-beam evaporation system, with a standard lift-off process in *N*-methylpyrrolidone (nmp) being performed to create the Cr capping layer that was used in the reactive-ion etching (RIE) as a hard mask in both cases. The RIE process was carried out in 16 sccm SF_6 and 12 sccm CHF_3 at approximately 140 W, and under a pressure of 18 mTorr. These conditions resulted in an anisotropic etch that enabled the formation of the straight sidewalls on the nanopillars discussed here [23]. After RIE, the Cr etch mask was stripped using a wet chemical etchant. The sample to be used to probe the role of the combined LSP and PSP was overcoated with 50 nm of Au via e-beam evaporation after fabrication of the Si nanopillars to produce both a Au cap on top of the Si nanopillars and a uniform Au film coating the base area of the arrays. This sample will henceforth be referred to as the "Au cap-film." The base film on this sample covered the entire surface of the sample, including the regions between the Si nanopillars, with the exception of a 5–10 nm air-gap ring that surrounded the periphery of each nanopillar. Thus, this film can be envisioned as having a periodic array of circular perforations, analogous to an extraordinary transmission grating and can be referred to as an array of nanoholes. In Fig. 1a, a ×5 optical image of the full-array set on the Au cap-film sample is labeled with the corresponding average values, before Au deposition, for nanopillar diameters (increasing vertically, from bottom to top) and interpillar gaps (increasing horizontally, from right to left) for arrays on each row and column, respectively. The standard deviation for the average values on every row/column was found to be less than ±3 nm. The variations in color seen between the various arrays seen in Fig. 1a can be attributed to both diffraction and plasmonic absorption effects as discussed in the literature [23, 24]. Figure 1b shows a scanning electron microscope (SEM) image of a single 100×100 element array of nanopillars to illustrate the high uniformity in the resultant samples. It is important

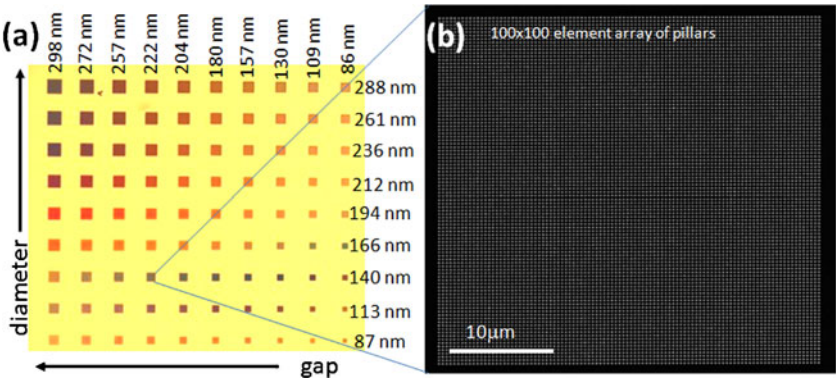

Fig. 1 **a** Optical microscopy image of the complete set of nanopillar arrays with varying nanopillar diameter and interpillar gap. The labels depict the increasing values in nanopillar diameter (*rows*) and gap (*columns*) for each array. **b** SEM image of a single 100×100 nanopillar array

to note that while some Au "beads" were deposited on the nanopillar sidewalls, as illustrated in the TEM image of a similar structure reported previously [23], the size of these irregular features varied between 10 and 30 nm. Although the impact on the overall enhancement factor of such discontinuous Au growth on the nanopillar sidewalls is not clearly understood, their random size and location throughout all the arrays suggests that their effect on identifiable patterns (diameter dependence, for instance) in the measured enhancement factors is minimal. This is also supported by simulation results previously reported [23].

The sample in which only LSP were expected, henceforth referred to as the "Au cap-only" sample, was fabricated by depositing a 50 nm Au film via e-beam evaporation followed by a 30 nm Cr evaporation prior to liftoff. Following liftoff and subsequent RIE, this left a Au cap on top of the Si nanopillar with a thin Cr cap on top of the Au. The Cr was removed via a wet-chemical etchant leaving behind the remaining Au cap without an underlying Au film. SEM images of the (a) bare (before Au deposition), (b) Au cap-film, and (c) Au cap-only Si nanopillars are presented in Fig. 2. The insets on the top right corner of each of the SEM images are the corresponding 3D schematic diagrams for each sample. The Au coverage of the pillar cap and base (when present) was approximately 45 nm thick.

SERS Measurements

It is well-known that the SERS intensity is directly correlated to the measurements of the surface plasmon resonance (SPR) spectra as the plasmonic fields near the surface of the nanoparticles being probed are the same fields that enhance the Raman signal of molecules that are adsorbed onto the metal nanostructures [25–28]. In fact, Jackson et al. [26], among other research groups, have used the wavelength dependence of the SERS signal to map out the spatial distribution of plasmonic fields in nanoparticles. Here we used an analogous approach where we have modified the diameter of our structures over a large range to monitor where the optimal response occurred under 785 nm excitation conditions. From our simulations (not shown), and due to the lower Raman efficiency at longer incident wavelengths, it was expected that this incident fell within the wavelength range where the optimal response would be observed. Furthermore, these simulations allowed us to

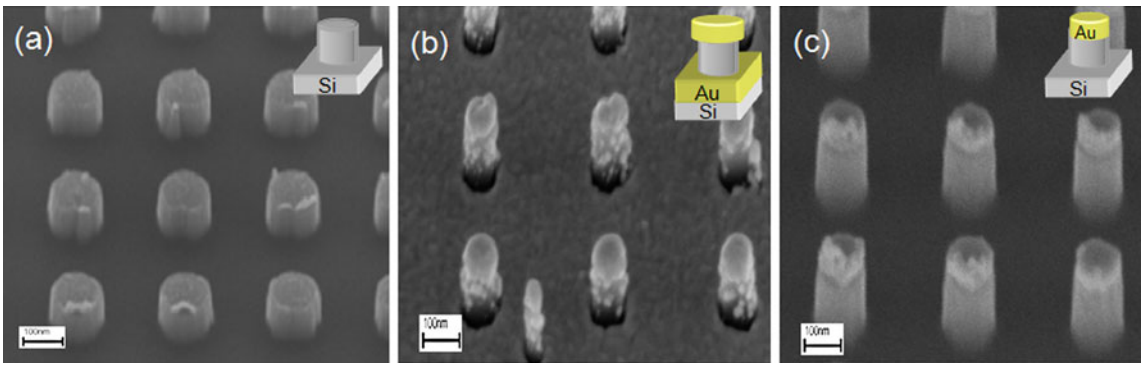

Fig. 2 SEM images of the nanopillar arrays. The images show **a** uncoated Si nanopillars, **b** e-beam Au-coated Si nanopillars corresponding to the Au cap-film sample, and **c** Si nanopillars from the Au cap-only sample. The *insets* on each figure displays a schematic representation of the ideal case of the corresponding structure of each sample

determine the nature of the plasmons participating in the plasmonic fields and, in turn, the expected SERS enhancement. For that reason, both of our samples were functionalized with thiophenol after their fabrication and, subsequently, SERS measurements at 785 nm incident were performed. In this case, the self-assembled monolayer was created by immersing the final Au-coated nanostructures in a 1×10^{-3} M solution of thiophenol in ethanol for 18 h. A direct comparison between the enhancement factor as a function of nanopillar diameter and gap for both samples was found to provide a clear picture of the role of both the LSP and PSP in SERS, as well as offering valuable insight into the mechanism describing LSP and PSP behavior within such nanostructures.

The SERS spectra of each nanopillar array were collected using a DeltaNu ExamineR μ-Raman system. The power of the 785-nm excitation source was 8.2 mW. The laser was focused to a size of 2 μm on the sample surface through a ×50, 0.75 NA objective. The back-reflected light was collected using a thermoelectrically cooled CCD array detector. Due to significantly more intense SERS signal observed for the Au cap-film sample, the data was collected with acquisition times of 2 s, while the collection time for the cap-only sample was 10 s. After data collection, the enhancement factor of the collected spectra were calculated taking into account the exposed Au surface coverage on the array area, nanostructure geometry, surface density of the thiophenol molecule in a self-assembled monolayer, the incident laser spot size, power, and integration time. More specifically, the enhancement factor G is defined as

$$G = \left(\frac{I^{\mathrm{SERS}}/N^{\mathrm{SERS}}}{I^{\mathrm{Raman}}/N^{\mathrm{Raman}}}\right);$$

where I^{SERS}, I^{Raman}, N^{SERS}, and N^{Raman} are the SERS and Raman intensities in counts and the number of probed molecules in the SERS and Raman measurements, respectively. I^{SERS} reflects the incident power P and integration time t corrections as $I^{\mathrm{SERS}} = I^{\mathrm{SERS-coll.}}/(t\times P)$. N^{SERS} is the calculated number of thiophenol molecules probed via the SERS process, assuming monolayer coverage of the Au surface. I^{Raman} and N^{Raman} are the corresponding calculation accounting for P and t corrections of the measured Raman intensities and number of probed molecules, respectively, during collection of the neat spectra. For the most accurate calculation of the SERS enhancement, it is of the utmost importance to have a uniform and well-defined molecular surface coverage. While many experiments in the SERS community have focused on free molecules such as Rhodamine 6G [29], the treatment of the SERS-active surface with low-concentration solutions of such molecules will inevitably lead to random distributions with high and low densities dispersed throughout the detection region, thereby providing unclear results. Therefore, the use of SERS-active, self-assembled monolayers are preferred, as these provide a known surface coverage, thus providing an accurate depiction of the number of molecules participating within a given SERS experiment [23, 30]. The surface coverage for thiophenol has been reported in the literature as 0.544 nmol/cm^2 [31–33]. Additional information about the experimental setup used here and a full discussion of the enhancement factor calculations can be found in the literature [23, 24, 34].

Results and Discussion

Experimental Results

In Fig. 3, we present μ-Raman spectra collected from nanopillar arrays with a post-Au diameter of 145 nm and an interpillar gap of 196 nm on the Au cap-film sample (red line) and the Au cap-only sample (blue line). Both spectra shown were corrected to account for both the laser power and acquisition time. It is important to note that although there is significant variation in the intensity of the SERS bands and the underlying photoluminescence of both spectra, the Raman band positions and relative intensities between the peaks remained consistent throughout measurements on arrays where SERS was observed. The 998 cm^{-1} band, which is attributed to the C–H wagging mode of thiophenol molecules, was used to calibrate the enhancement factor of the SERS response for each array in both samples. This mode was chosen as the C–H bonds are

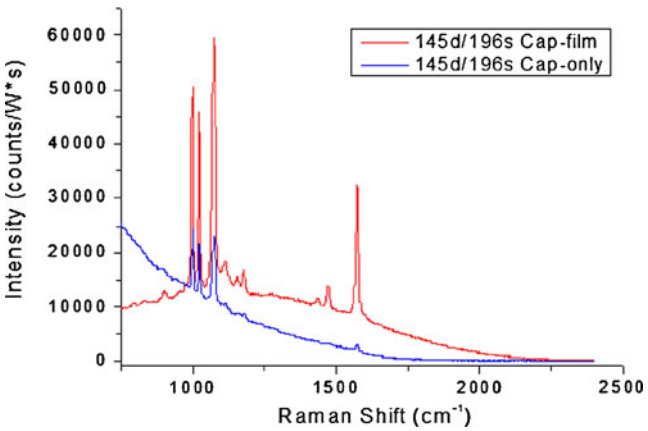

Fig. 3 SERS spectra from nanopillar arrays with diameter of 145 nm and gap of 196 nm on the Au cap-film (*red*) and Au cap-only (*blue*) samples. The power of the 785-nm incident laser remained the same on both measurements. The data were corrected to account for differences in acquisition time. The intensity of the 998 cm^{-1} band is significantly higher on the cap-film SERS spectrum. There is also a marked variation on the underlying photoluminescence of the two samples

the furthest removed from the S-metal bond, which is known to induce hybridized states within the molecular HOMO–LUMO gap, and therefore can modify the polarizability of the molecule near that bond, thus affecting the Raman intensity in addition to any SERS-based changes [35]. As such, the SERS response of the 998 cm^{-1} mode compares most directly with the neat spectrum of thiophenol as only plasmonic effects should influence the response, thereby separating out or at least limiting any additional enhancements due to changes in polarizability or resonant Raman effects from the hybridized states.

In Fig. 4a, b, we present spatial plots of the SERS enhancement factor as a function of nanopillar diameter and interpillar gap for the cap-film and cap-only samples, respectively. The corresponding average values following Au deposition for the diameters (rows) and interpillar gaps (columns) of each array on the two samples are presented on the *y*- and *x*-axes of Fig. 4a and b, respectively. In these plots, each pixel refers to the enhancement factor for a given array, with interpolation through Microcal Origin® providing the smoothing of the dependences on gap and diameter. It was determined previously that the standard deviation in the SERS response across an entire array was always less than 30%, and more typically falling in the 15% range, thus we arbitrarily chose the center of each array as the probed location on all arrays, with the knowledge that this was representative of the SERS intensity of the entire array [34]. The plots presented in Fig. 4 indicate that there is a strong dependence of the SERS enhancement factor upon the nanopillar diameter, while only a monotonic increase in SERS response was observed with increasing interpillar gap, as discussed previously for Au cap-film samples by Caldwell et al. [24]. However, upon comparing the relative plots for the two samples discussed here, it is clear that the presence of the film, while only minimally influencing the diameter and gap responses, does induce a large increase in the SERS enhancement factor of over an order of magnitude at the optimal diameter (on resonance) and over 2 orders of magnitude at most other diameters (off resonance). The significant effect of the film on the enhancement factor is more clearly seen in Fig. 4c, where the fractional enhancement factor relative to the Au cap-only sample, $(G_{cap\text{-}film}-G_{cap\text{-}only})/G_{cap\text{-}only}$, where $G_{cap\text{-}film}$ and $G_{cap\text{-}only}$ are the enhancement factors of the Au cap-film and Au cap-only samples, respectively, is plotted as a function of nanopillar diameter and interpillar gap. Such a peak in the SERS response at a given diameter can be understood as follows: (1) at small-diameter structures, the SPR lies at a wavelength below the incident photon and Raman scattered photon energies, thus a weak SERS response is observed; (2) as the diameter is increased, eventually, such a diameter is reached where the SPR peak coincides with the energy of the incident and/or Raman scattered photons, thereby providing the largest SERS enhancement; (3) further increasing the pillar diameter induces a further red shift in the SPR condition to an energy beyond the Raman spectral window, thus resulting in a decrease in the SERS enhancement.

In addition to the increases in peak SERS response both on and off resonance, the diameter dependence is also observed to be significantly broadened when the nanohole array (Au film at the base of the nanopillars) is present, as observed by comparing the spatial maps in Fig. 4a, b. This is consistent with the broadening of the SPR curve that is predicted when PSP are present [20], which in turn would broaden the range of diameters where the SPR and Raman spectral window coincide. The observed increases and broadening in the SERS response for samples with the Au film indicates that not only does the film increase the sensitivity of the detection, while not modifying the optimal array/nanopillar geometries, but also enables a broadening of the SPR condition, which leads to more "forgiving"

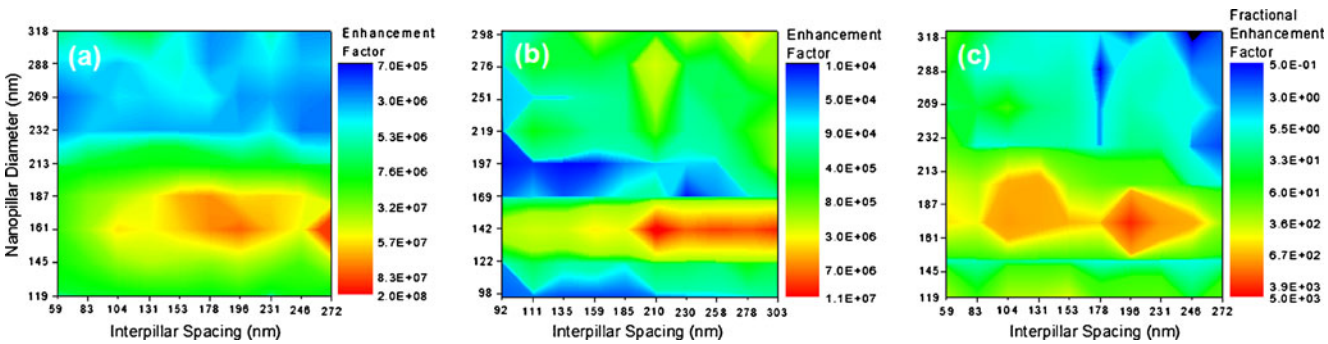

Fig. 4 Enhancement factor contour maps of **a** the Au cap-film sample and **b** the Au cap-only sample. The *labels* on the *x*- and *y*-axis illustrate the increasing average values in nanopillar diameter (*rows*) and gap (*columns*) for each array. The Au cap-film map presents an order of magnitude improvement in enhancement factor at optimal nanopillar diameter and gap and a broadened response when compared to the maximum value and response linewidth obtained for the Au cap-only map. **c** Fractional enhancement factor relative to the Au cap-only sample plotted as a function of nanopillar diameter and interpillar gap

architectures. These results reveal a maximum enhancement factor of approximately 2.0×10^8 for the Au cap-film system as discussed by Caldwell et al. [24] and 1.1×10^7 for the Au cap-only arrays. These results also show higher enhancement factors than previously reported by Baumberg et al. [30] for periodic nanohole arrays in which enhancements of 3.0×10^6 were observed. Even lower enhancement factors were reported by Yu et al. [36, 37] for periodic nanohole and nanodisk arrays that were fabricated via e-beam lithography from which values of 4.2×10^5 and 1.3×10^3, respectively, were measured. One important point to consider is that although enhancements factors of 1.0×10^9 have been reported for Au-coated nanopillars that are aperiodically arranged [29] however, as stated previously, it is difficult to accurately predict the enhancement factor for systems with inherently random molecular and plasmonic nanoparticle distributions.

As mentioned above, in addition to the higher SERS enhancement detected from the Au cap-film sample, the bandwidth of the response is also significantly broader, as shown in Figs. 3 and 4. This result strongly suggests PSP–PSP interactions within the thin Au film. The evanescent nature of the EM near-fields inside the Au cap-film sample will produce PSP modes at both the Au-air interface on the surface of the structure and at the Au-Si substrate interface for Au films below a particular thickness threshold of approximately 40 nm [20]. HRTEM measurements on our samples revealed that the film thickness was approximately 40–45 nm thick, which is in the range of this threshold. In this case, the interactions between the PSP located at each of the two interfaces in the gold film can induce a break in the degeneracy of the PSP states similar to the same-energy level repulsion concept of the bonding–antibonding model in molecular physics [38], thereby causing a broadening of the SPR response [20, 39]. In addition, as the SERS enhancement is determined by the product of the square of the SP EM near-field intensities at the relative positions in frequency space of the incident laser line and the SERS vibrational mode of interest, a broadening in the SPR condition will be expected to manifest itself as a broadening in the optimal diameter under the measurement conditions reported here. Given that such interactions do not significantly modify the center of the SPR peak [20, 24] and that both the incident and detection frequencies are constant in all experiments reported here, a broadening of the SPR condition will enable a wider range of nanopillar diameters to have significant overlap between the SPR condition and the incident and detection frequencies.

Theoretical Simulations

Simulations performed using the COMSOL MultiPhysics software package also qualitatively support the results presented and conclusions drawn here. Presented in Fig. 5 is the spectral response of the calculated enhancement factor values of both Au cap-film (solid lines) and Au cap-only (dashed lines) nanopillar arrays with 100 nm inter-pillar gaps in a semi-infinite array using periodic boundary conditions. The graph compares the calculated SERS response of arrays of nanopillars with diameters 100, 150, and 200 nm (blue, red, and green traces, respectively) for each of the two types of arrays under study. For the simulations reported the diameter refers to the diameter of the Si nanopillars, with the cap-film structure having an additional 13 nm increase in the radius of the Au cap due to the mushroom-shaped cap and the associated overhang. The height of the Si nanopillars was 170 nm. From the graph, it is clear that there is at least an order of magnitude increase in the enhancement factors at almost all wavelengths where enhancements are observed for the cap-film structure with respect to the cap-only samples. Such increases in SERS enhancement in the presence of the Au film is in good agreement with the experimental results presented here. In addition, the SERS spectral response of the cap-film sample was observed to be significantly broader at all diameters studied in comparison to those of the cap-only nanopillar arrays. An important difference between the results from both samples is that the peaks of the cap-film response do not shift significantly in spectral position with varying nanopillar diameter, while significant red shifts in the highest intensity peak in the SERS spectral response were observed as the nanopillar diameter was

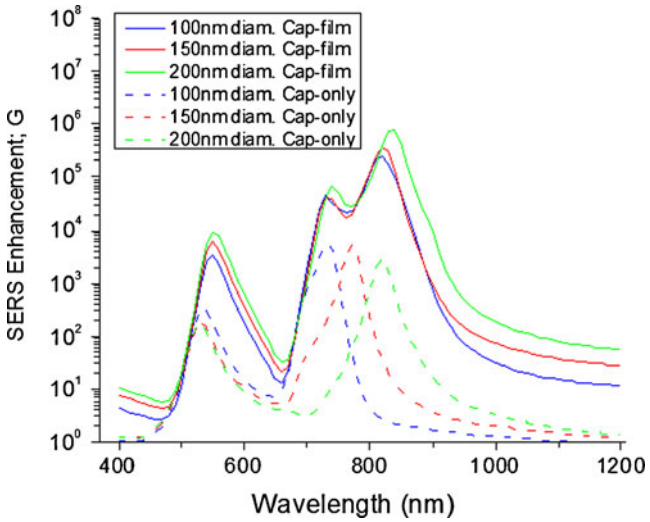

Fig. 5 Simulation results showing the enhancement factor G plotted as a function of incident wavelength from the Au cap-film (*solid lines*) and Au cap-only (*dashed lines*) samples for nanopillar arrays with diameters, defined as double the radius of the top surface of the Si nanopillars, of 100 (blue), 150 (*red*), and 200 (*green*)nm. There is at least approximately an order of magnitude increase in enhancement factor for the cap-film sample with a significantly broader bandwidth on all spectral peaks when compared to the cap-only sample

increased in the cap-only sample. In comparison, the cap-only calculations exhibited a red shift in the peak center frequency from approximately 730 to 820 nm when the diameter was increased from 100 to 200 nm. However, although the calculated relative variation in enhancement intensity between the two samples are in good qualitative agreement with the experimental results, the observed enhancement factors differ from the simulations results by approximately 2–3 orders of magnitude. Some of this variation can be accounted for by chemical enhancement effects that are not accounted for in our simulations. It is now widely known that chemical enhancement plays a significant role in the amplification of the SERS intensity of adsorbed molecules on noble metals [23, 40].

An important point to consider is the possible effect that the Au clumps that are randomly located along the sidewalls of the nanopillars may have on the overall enhancement observed from the Au cap-film sample. Although Hu et al. [41] have reported a significant effect on the enhancement observed due to of the presence of nanodots attached to the sidewalls of SiO_2 nanopillars, the degree to which these small clumps impact the enhancement factors, the mechanism by which they cause such variations and their dependence on particle position, geometry, number, etc., remains unclear. Therefore, the possibility of Au nanodots around the sidewalls of the nanopillar arrays playing a significant role in the enhancement mechanism of the arrays should not be discarded. It may be possible that these nanometer-sized clumps can produce a cooperative effect in which their impact may be two-fold. First, they may increase enhancement factors by producing higher EM fields in their vicinity. Second, they could also function as intermediaries between the LSP at the top surface of the nanopillars and PSP near the nanopillar base thereby altering the SPR spectrum of the arrays. However, it is important to note that the results reported here do not support a model in which the nanodots on the sidewalls have a significant impact on SERS measurements for 785 nm incident. As illustrated in Fig. 4, a dramatic dependence on the nanopillar diameters is observed for both samples, whereby nanopillars with and without such nanodots are observed, thus ruling out any major influence of the nanodots on the reported enhancement factors. In addition, given that the nanodots were consistently observed to be attached to the nanopillar sidewalls at random locations on all arrays of the Au cap-film sample, a large impact on their enhancement factors would be expected to have resulted in large enhancements on arrays at random locations on the samples and the SERS measurements would have exhibited little or no diameter dependence, instead of providing a dependence more or less mirroring that of the Au cap-only structures where such nanodots were absent. Furthermore, one would expect that such randomly oriented nanodots would lead to a high degree of variability in the enhancement factor as a function of spatial location within a given array, and thus one would not anticipate standard deviations such as those observed here. Moreover, the measured sizes of the nanodots indicate that it is likely that the peak of their SPR spectrum lies around 530–600 nm, i.e., bulk SPR for Au [40], in contrast to the 785-nm incident used here. This is also consistent with Mie scattering calculations for Au spheres in air as well as additional COMSOL simulations [23] in which the presence of such nanodots at random locations on the sidewalls of the nanopillars induced large increases in the SERS enhancement in the range of 530–700 nm; however, no such increases were observed near 785 or 857 nm, which represents the wavelength of the incident photons and of the Raman scattered light at 998 cm^{-1}.

Conclusion

In conclusion, the results of this study show an increase in enhancement factor of 1–2 orders of magnitude for Si nanopillar arrays where both a Au cap and a Au film are present in comparison to those detected from similar nanopillars with only the Au cap. The enhancement factors at optimal diameters observed are 2–3 orders of magnitude higher than values previously reported for nanohole arrays and 5 orders of magnitude higher than those previously reported for nanodisk arrays. The range of diameters at which higher enhancement factors are observed is also broader for the Au cap-film structures, which suggests non-trivial interactions between the localized (LSP; located at the Au cap) and propagating (PSP; Au film) surface plasmons. These results are in good qualitative agreement with EM field simulations where a higher enhancement and larger bandwidth of the SPR condition is obtained for the systems where both LSP and PSP are present.

Acknowledgments The authors would like to thank Drs. Doewon Park and Robert Bass for their advice involving e-beam lithography. We also would like to express our thanks to Drs. James Long and Jeff Owrutsky for their helpful discussions. We also recognize the Center for Nanoscale Science and Technology at NIST in Gaithersburg, MD, USA, for the electron-beam lithography. The authors recognize funding support through the Naval Research Laboratory's Nanoscience Institute. F. J. Bezares acknowledges the support of the American Society of Engineering Education Postdoctoral Fellowship Program.

References

1. Fleischmann M, Hendra PJ et al (1974) Raman spectra of pyridine adsorbed at a silver electrode. Chem Phys Lett 26(2):163–166
2. Jeanmaire RP, van Duyne J (1977) Surface-enhanced electrochemistry. Electroanal Chem (Elsevier Sequouia SA) 84:1–20

3. Moskovits M (1985) Surface-enhanced spectroscopy. Rev Mod Phys 57(3):783–826
4. Kawata S, Inouye Y et al (2009) Plasmonic for near-field nano-imaging and superlensing. Nat Photon 3:388
5. Smolyaninov II, Davis CC et al (2009) Magnifying superlenses and other applications of plasmonic metamaterials in microscopy and sensing. Chemphyschem 10:625
6. Schuller JA, Barnard ES et al (2010) Plasmonics for extreme light concentration and manipulation. Nat Mater 9:193
7. Pala RA, White J et al (2009) Design of plasmonic thin film solar cells with broadband absorption enhancements. Adv Mater 21:3504
8. Lee JW, Seo JY et al (2005) Invisible plasmonic meta-materials through impedance matching to vacuum. Opt Express 13:10681
9. Kneipp K, Wang Y et al (1997) Single molecule detection using surface-enhanced Raman scattering. Phys Rev Lett 78(9):1667–1670
10. Jiang JK, Bosnick K et al (2003) Single molecule Raman spectroscopy at the junctions of large Ag nanocrystals. J Phys Chem B 107:9964
11. Nie S, Emory SR (1997) Probing single molecules and single nanoparticles by surface-enhanced Raman scattering. Science 275:1102–1106
12. Kalele SA, Tiwari NR et al (2007) Plasmon-assisted photonics at the nanoscale. J Nanophoton 1:012501
13. Maier SA, Atwater HA et al (2005) Plasmonics: localization and guiding of electromagnetic energy in metal/dielectric structures. J Appl Phys 98:011101
14. Ebessen TW, Genet C et al. (2008) Surface-plasmon circuitry. Physics Today (May) 44
15. Stockman MI, Faleev SV et al (2001) Localization versus delocalization of surface plasmons in nanosystems: can one state have both characteristics? Phys Rev Lett 87:167401
16. Dionne JA, Sweatlock LA et al (2010) Silicon-based plasmonics for on-chip photonics. IEEE J Sel Top Quant Electron 16:295
17. Barnes WL, Dereux A et al (2003) Surface plasmon subwavelength optics. Nature 424:824
18. Stuart HR, Hall DG (1998) Enhanced dipole-dipole interaction between elementary radiators near a surface. Phys Rev Lett 80:5663
19. Cesario J, Quidant R et al (2005) Electromagnetic coupling between a metal nanoparticle grating and a metallic surface. Opt Lett 30:3404
20. Papanikolaou N (2007) Optical properties of metallic nanoparticle arrays on a thin metallic film. Phys Rev B 75:235426
21. Chu Y, Crozier KB (2009) Experimental study of the interaction between localized and propagating surface plasmons. Opt Lett 34:244
22. Mock JJ, Hill RT et al (2008) Distance-dependent plasmon resonant coupling between a gold nanoparticle and gold film. Nano Lett 8(8):2245–2252
23. Caldwell JD, Glembocki OJ et al (2011) Plasmonic nanopillar arrays for large-area, high enhancemetn surface-enhanced Raman scattering sensors. ACS Nano 5(5):4046–4055
24. Caldwell JD, Glembocki OJ et al. (2010) Plasmo-photonic Nanowire Arrays for Large-Area Surface-enhanced Raman Scattering. Proc. of SPIE 7757:775723–1
25. Lu Y, Liu GL et al (2005) High-density silver nanoparticle film with temperature-controllable interparticle spacing for tunable surface enhanced Raman scattering substrate. Nano Lett 5(1):5–9
26. Jackson JB, Westcott SL et al (2003) Controlling the surface enhanced Raman effect via the nanoshell geometry. Appl Phys Lett 82(2):257–259
27. Laurent G, Felidj N et al (2005) Evidence of multipolar excitations in surface enhanced Raman scattering. Phys Rev B 71:1–6
28. Liu Y, Xu S et al (2010) Note: simultaneous measurement of surface plasmon resonance and surface-enhanced Raman scattering. Rev Sci Instrum 81:036105
29. Habouti S, Materfi-Tempfli M et al (2011) On-substrate, self-standing Au-nanorod arrays showing morphology controlled properties. Nano Today 6:12–19
30. Baumberg JJ, Kelf TA et al (2005) Angle-resolved surface-enhanced Raman scattering on metallic nanostructured plasmonic crystals. Nano Lett 5:2262–2267
31. Whelan CM, Smyth MR et al (1998) HREELS, XPS, and electrochemical study of benzenethiol adsorption on Au(111). Langmuir 15:116–126
32. Carron KT, Hurley LG (1991) Axial and azimuthal angle determination with surface-enhanced Raman spectroscopy-Thiophenol on copper, silver and gold metal-surfaces. J Phys Chem 95:9979–9984
33. Taylor CE, Pemberton JE et al (1999) Surface enhancement factors for Ag and Au surfaces relative to Pt surfaces for monolayers of thiophenol. Appl Spectrosc 53:1212–1221
34. Bezares F, Caldwell JD (2011) Plasmo-photonic nanopillar arrays for large-area surface-enhanced Raman scattering sensors. Proc of SPIE 7946:79461A-1
35. Alexson DA, Badescu SC et al (2009) Metal-adsorbate hybridized electronic states and their impact on surface-enhanced Raman scattering. Chem Phys Lett 477:144–149
36. Yu Q, Braswell S et al (2010) Surface-enhanced Raman scattering on gold quasi-3D nanostructure and 2D nanohole arrays. Nanotechnology 21:355301
37. Yu Q, Guan P et al (2008) Inverted size-dependence of surface-enhanced Raman scattering on gold nanohole and nanodisk arrays. Nano Lett 8:1923–1928
38. Halas NJ, Lal S et al (2011) Plasmons in strongly coupled metallic nanostructures. Chem Rev 111:3913–3961
39. Marquier F, Greffet JJ et al (2005) Resonant transmission through a metallic film due to coupled modes. Opt Express 13:70
40. Aroca R (2006) Surface-enhaced vibrational spectroscopy, 1st edn. Wiley, England
41. Hu J,Wen-Di L et al. (2010) Effects of nanodots on surface plasmons and electric field enhancement in nano-pillar antenna array. 2010 Conference on Lasers and Electro-optics 978-1-55752-890-2.